

MICROPLANE MODEL M4 FOR CONCRETE. I: FORMULATION WITH WORK-CONJUGATE DEVIATORIC STRESS

By Zdeněk P. Bažant,¹ Fellow, ASCE, Ferhun C. Caner,² Ignacio Carol,³
Mark D. Adley,⁴ and Stephen A. Akers⁵

ABSTRACT: The first part of this two-part study presents a new improved microplane constitutive model for concrete, representing the fourth version in the line of microplane models developed at Northwestern University. The constitutive law is characterized as a relation between the normal, volumetric, deviatoric, and shear stresses and strains on planes of various orientations, called the microplanes. The strain components on the microplanes are the projections of the continuum strain tensor, and the continuum stresses are obtained from the microplane stress components according to the principle of virtual work. The improvements include (1) a work-conjugate volumetric deviatoric split—the main improvement, facilitating physical interpretation of stress components; (2) additional horizontal boundaries (yield limits) for the normal and deviatoric microplane stress components, making it possible to control the curvature at the peaks of stress-strain curves; (3) an improved nonlinear frictional yield surface with plasticity asymptote; (4) a simpler and more effective fitting procedure with sequential identification of material parameters; (5) a method to control the steepness and tail length of postpeak softening; and (6) damage modeling with a reduction of unloading stiffness and crack-closing boundary. The second part of this study, by Caner and Bažant, will present an algorithm for implementing the model in structural analysis programs and provide experimental verification and calibration by test data.

INTRODUCTION

The classical approach to the constitutive modeling of concrete, in which the material model is formulated directly in terms of stress and strain tensors and their invariants, has led at the beginning of the computer era to important advances. But, at present, this approach has probably entered a period of diminishing returns, in which a great effort yields only minor and insufficient improvements to the constitutive model. Much more promising and conceptually transparent is the microplane model, in which the constitutive law is formulated in terms of vectors rather than tensors—as a relation between the stress and strain components on a plane of any orientation in the material microstructure, called the microplane (Bažant 1984; see Appendix I). Microplanes of many spatial orientations, related to the strain and stress tensors by a kinematic constraint and a variational principle, are considered. The microplane model can be seen as a consequence of the hypothesis that the free energy density of the material is a sum of the free energy densities expressed as functions of the strain vector on planes of various orientations (Carol et al. 1999).

The background of the microplane modeling approach, described in more detail in Bažant et al. (1996a), can be traced back to a pioneering idea of the great G. I. Taylor (1938) dealing with plasticity of polycrystalline metals. Taylor's idea was formulated in detail by Batdorf and Budianski (1949) and became known as the “slip theory of plasticity.” This theory

was soon recognized as the most realistic constitutive model for plastic-hardening metals. It was refined in a number of subsequent works (e.g., Kröner 1961; Budianski and Wu 1962; Hill 1965, 1966; Lin and Ito 1965, 1966; Rice 1970). It was used in arguments about the physical origin of strain hardening and was shown to allow easy modeling of anisotropy as well as the vertex effects for loading increment to the side of a radial path in stress space. All the formulations considered that only the inelastic shear strains (“slips”), with no inelastic normal strain, were taking place on what is now called the “microplanes.” The theory was also adapted to anisotropic rocks under the name “multilaminate model” (Zienkiewicz and Pande 1977; Pande and Sharma 1981, 1982; Pande and Xiong 1982).

All these models assumed the planes of plastic slip in the material (in those studies called the “slip planes” and here called the “microplanes”) to be constrained statically to the stress (“macrostress”) tensor σ_{ij} (i.e., the stress vector on each “microplane” was the projection of σ_{ij}). The elastic strain was not included on the slip planes but was added to the inelastic strain tensor on the continuum level (macrolevel). Strain softening was not of interest in the aforementioned studies, but even if it were, it could not have been modeled (Bažant 1984) because under the static constraint a strain-softening constitutive law for the microplane makes the material unstable even if ϵ_{ij} is prescribed.

PREDECESSORS OF PRESENT MODEL

The original objective was to model strain softening leading to fracture and to include inelastic volume changes, especially dilatancy due to shear. In the first microplane model presented at a 1983 Tucson conference, labeled M1⁰ (Bažant 1984), this objective was found to require four new features departing from the basic characteristics of the previous slip theory models for metals and rocks: (1) The static “micro-macro” constraint was found to cause instability of the microplane system in postpeak strain softening, and to cure it, it was found necessary to impose a kinematic “micro-macro” constraint in which the strain vector on each microplane is the projection of the strain tensor ϵ_{ij} [the possibility of such a constraint had also been suggested by G. I. Taylor (1938), but remained unexplored up to 1983]. (2) As a consequence of the kinematic constraint, it was found necessary to include the elastic strains on the microplane level, and not as added strains on the mac-

¹Walter P. Murphy Prof. of Civ. Engrg. and Mat. Sci., Northwestern Univ., McCormick School of Engrg. & Appl. Sci., 2145 Sheridan Rd., Evanston, IL 60208. E-mail: z-bazant@northwestern.edu

²Grad. Res. Asst., Northwestern Univ., 2145 Sheridan Rd., Evanston, IL.

³Prof., Universidad Politecnica de Catalunya, Jordi Girona 1–3, Edif. D2, E-08034, Barcelona, Spain; formerly Visiting Scholar, Northwestern Univ., Evanston, IL.

⁴Res. Civ. Engrg., U.S. Army Engineer Waterways Experiment Station, Geomechanics Div., 3909 Halls Ferry Rd., Vicksburg, MS 39180.

⁵Res. Civ. Engrg., U.S. Army Engineer Waterways Experiment Station, Geomechanics Div., 3909 Halls Ferry Rd., Vicksburg, MS.

Note. Associate Editor: Gilles Pijaudier-Cabot. Discussion open until February 1, 2001. Separate discussions should be submitted for the individual papers in this symposium. To extend the closing date one month, a written request must be filed with the ASCE Manager of Journals. The manuscript for this paper was submitted for review and possible publication on March 2, 1999. This paper is part of the *Journal of Engineering Mechanics*, Vol. 126, No. 9, September, 2000. ©ASCE, ISSN 0733-9399/00/0009-0944–0953/\$8.00 + \$.50 per page. Paper No. 20387.

rocontinuum level. (3) Instead of a simple superposition of the inelastic strains on all the slip planes, as used in the previous models, it was found necessary to introduce a variational principle (principle of virtual work) in order to relate the stresses on the microplanes of all possible orientations to the macrocontinuum stress tensor (and thus ensure equilibrium). (4) While the previous models considered only plastic slips, model M1⁰ introduced normal inelastic strains on the microplanes, which made it possible to simulate not only plasticity but also multidirectional distributed tensile cracking (for more detail, see Appendix I).

The neutral term “microplane” was coined to reflect the fact that the model is not restricted to plastic slip (the prefix “micro,” of course, does not imply actual simulation of the microstructure geometry, but merely alludes to a separate characterization of the inelastic deformations on planes of various orientations within the microstructure).

Each microplane was endowed in model M1⁰ with a 2D inelastic constitutive law based on a loading surface relating the normal and shear strain components on the microplane, and also with a loading potential (with a nonassociated flow rule for the inelastic stress decrements). However, the use of multidimensional loading surfaces on the microplane level was later found to be an unnecessary complication for data fitting, contrary to the simple philosophy of the microplane model. Therefore, the subsequent microplane models involve on the microplane level only simple one-to-one relations between one stress component and the associated strain component, with no cross dependencies. Except for pure friction, macroscopic cross effects such as dilatancy are automatically generated by interactions among various microplanes, which seem to be adequately captured by the kinematic constraint, as comparisons with tests later demonstrated. No test data have been fit with model M1⁰.

The subsequent development at Northwestern of practically applicable and experimentally calibrated microplane models for concrete can in retrospect be divided into four stages, resulting in models now labeled as M1 through M4. All these models have the aforementioned four features.

Model M1 (Bažant and Oh 1983, 1985), in view of the lack of success in using M1⁰ to describe both tension and triaxial compression, was focused only on tensile failure. It simulated smeared multidirectional tensile cracking and postpeak tensile softening of concrete, which it represented as well as, or better than, any other multidirectional smeared cracking model or continuum damage model. Model M1 considered only the normal microplane stresses, defined as nonlinear hardening-softening functions of the normal microplane strains. When the microplane shear stress components are absent, Poisson’s ratio ν is fixed as 1/4 (or 1/3) in three (or two) dimensions, respectively, while for concrete $\nu \approx 0.18$. Therefore, Poisson’s ratio was adjusted by coupling in series with the microplane system an elastic element exhibiting only a volumetric strain. For calculating the macrostresses from microplane stresses, optimum Gaussian integration on a spherical surface was introduced and some new effective integration formulae developed (Bažant and Oh 1986).

In tandem with the crack band concept, model M1 is capable of representing well all the fracture tests of notched concrete specimens, including the size effect, and was also extended to fit well the basic data on dilatant shear on preexisting cracks in concrete (Bažant and Gambarova 1984). For the modeling of compression, a compressive strength limit on the normal microplane strain could not be imposed because compression failure would then also occur under hydrostatic pressure or uniaxial strain loading. Model M1 nevertheless did exhibit failure under uniaxial compression (it was triggered when lateral expansion due to the Poisson effect caused tensile

failure on the microplanes roughly parallel to the direction of compression). However, the compression strength was far too high and a snapback occurred immediately after the peak stress. To avoid it, an attempt was made to include shear stresses on microplanes, but the test data for uni-, bi-, and triaxial compression with volume expansion still could not be fit.

Model M2 (Bažant and Prat 1988a) and its several extensions (Bažant and Ožbolt 1990, 1992; Carol et al. 1992; Ožbolt and Bažant 1992, 1996), achieved the goal of simultaneous modeling of tensile and compressive failures by introducing a volumetric-deviatoric split of the normal strains and stresses on the microplanes. While the tensile failure is basically a uniaxial behavior, describable simply by a scalar relation between the normal stress and strain, compression failure is a triaxial phenomenon, in which failure is triggered by lateral expansion and by slip on inclined planes. The volumetric-deviatoric split helps to control these triaxial aspects. With this split, compression failure can be triggered not only by lateral expansion due to the Poisson effect, but also by lateral expansion due to high inelastic deviatoric strain on the microplanes parallel to the direction of compression or by slip on inclined microplanes.

Another advantage of the volumetric-deviatoric split is that Poisson’s ratio can have any value between -1 and 0.5 , as transpired from the relations of Young’s modulus and Poisson’s ratio to the microplane elastic constants worked out in Bažant and Prat (1988a) (if only elastic normal and shear strains on the microplane level, with no split, are considered, then only Poisson’s ratios between -1 and 0.25 can be obtained).

An explicit reformulation of model M2 was presented by Carol et al. (1992). An efficient implementation of model M2 in a large dynamic explicit finite-element program was described by Cofer and Kohut (1994). A nonlocal generalization of model M2 was developed to prevent spurious excessive localization of damage in structures and spurious mesh sensitivity (Bažant and Ožbolt 1990; Ožbolt and Bažant 1992, 1996).

Model M2 was able to fit well the basic types of test data for uni-, bi-, and triaxial compression, axial-torsional tests, and tensile tests, but the long softening tails were not represented well (in retrospect, one problem was the lack of work-conjugacy of volumetric stress). A similar representation of test data was also achieved by a more complicated variant, M2^h, of model M2 (Hasegawa and Bažant 1993), which, instead of the volumetric-deviatoric split, used the normal strains in directions parallel to the microplane to simulate lateral expansion in compression failure.

Model M3 [Bažant et al. (1996a,b); see also Bažant and Planas (1998), Sect. 14.1] introduced the concept of stress-strain boundaries (or softening strain-dependent yield limits) on the microplane level. In this concept the microplane response is elastic until any of the boundaries is reached. If any of the boundaries is exceeded, the stress is made to drop at constant strain to the surface. Aside from simplicity and clarity, the advantage of this approach is that several independent boundaries for different stress components can be defined as functions of different strain components. This is helpful for simultaneous modeling of tensile, compressive, and shear softening.

A softening stress-strain curve for shear employed in model M2 was replaced in model M3 by a strain-independent linear frictional-cohesive yield surface relating the normal and shear stress components on the microplane. Introduction of an additional softening tensile stress-strain boundary for tension in Model M3 corrected a problem with the volumetric-deviatoric split in model M2 found in numerical simulations by M. Jir-

ásek (1993). Model M2 gave excessively large positive lateral strains in the tail of softening under uniaxial tensile stress. This was caused in M2 by localization of tensile strain softening into the volumetric strain, while the deviatoric strains on the strain-softening microplanes went into unloading.

Model M3 was also extended to moderately large finite strains. A method of scaling the parameters of the model to achieve the desired peak stress and strain at peak stress was formulated, the model parameters being divided into a few adjustable ones and many nonadjustable (or fixed, hard-to-adjust) ones, common to all concretes. A simplified way to filter out the size effect from test results and to delocalize the data from test specimens that suffered localization of damage has been formulated. The model was implemented in a large dynamic finite-element program by Cofer and Kohut (1994).

Model M4, which is mathematically formulated in the first part of this study. A number of further improvements are made, including a work-conjugate definition of the volumetric-deviatoric split [based on Carol et al. (1998)], improved formulations of boundary surfaces, frictional yield limits and damage, sequential identification of material parameters by data fitting, and a capability to control various response features by material parameters (see also Appendix I). Formulation of a numerical algorithm, experimental calibration, and application examples are relegated to the second part of this study (Caner and Bažant 2000). Two follow-up papers further extend model M4 to strain-rate sensitivity or creep and to arbitrarily large finite strain. A thermodynamic formulation based on potentials is formulated in two other studies (Carol et al. 2000; Kuhl and Carol 2000).

A series of microplane models have also been developed for the creep of anisotropic clay (Bažant and Kim 1986; Bažant and Prat 1987) and for the inelastic behaviors of soil (Prat and Bažant 1991) and rock (Prat et al. 1997). They share many features with the models for concrete.

REVIEW OF BASIC RELATIONS OF MICROPLANE MODEL

The classical constitutive models represent properly invariant equations directly relating the components σ_{ij} and ϵ_{ij} of the stress and strain tensors $\boldsymbol{\sigma}$ and $\boldsymbol{\epsilon}$ (the Latin lower-case indices refer to the components in Cartesian coordinates x_i ; $i = 1, 2, 3$). The microplane constitutive model is defined by a relation between the stresses and strains acting on a plane called the microplane, having an arbitrary orientation characterized by its unit normal n_i . The basic hypothesis, which ensures stability of postpeak strain softening (Bažant 1984), is that the strain vector $\boldsymbol{\epsilon}_N$ on the microplane [Fig. 1(a)] is the projection of $\boldsymbol{\epsilon}$, i.e., $\boldsymbol{\epsilon}_N = \boldsymbol{\epsilon}_{ij}n_j$. The normal strain on the microplane is $\epsilon_N = n_i\epsilon_{N_i}$, that is

$$\epsilon_N = N_{ij}\epsilon_{ij} \quad (1)$$

where $N_{ij} = n_i n_j$ (repetition of the subscripts, referring to Cartesian coordinates x_i , implies summation over $i = 1, 2, 3$).

The shear strains on each microplane are characterized by their components in directions M and L given by orthogonal unit coordinate vectors \vec{m} and \vec{l} , of components m_i, l_i , lying within the microplane. Vector m_i may, for example, be chosen to be normal to axis x_3 , in which case $m_1 = n_2(n_1^2 + n_2^2)^{-1/2}$, $m_2 = -n_1(n_1^2 + n_2^2)^{-1/2}$, $m_3 = 0$, but $m_1 = 1$ and $m_2 = m_3 = 0$ if $n_1 = n_2 = 0$. A vector m_i normal to x_1 or x_2 may be obtained by permutations of the indices 1, 2, and 3. The orthogonal unit vector is generated as $\vec{l} = \vec{m} \times \vec{n}$. To minimize directional bias, vectors \vec{m} are alternatively chosen normal to axes x_1, x_2 , or x_3 . The shear strain components in the directions of \vec{m} and \vec{l} are $\epsilon_M = m_i(\epsilon_{ij}n_j)$ and $\epsilon_L = l_i(\epsilon_{ij}n_j)$, and by virtue of the symmetry of tensor ϵ_{ij} ,

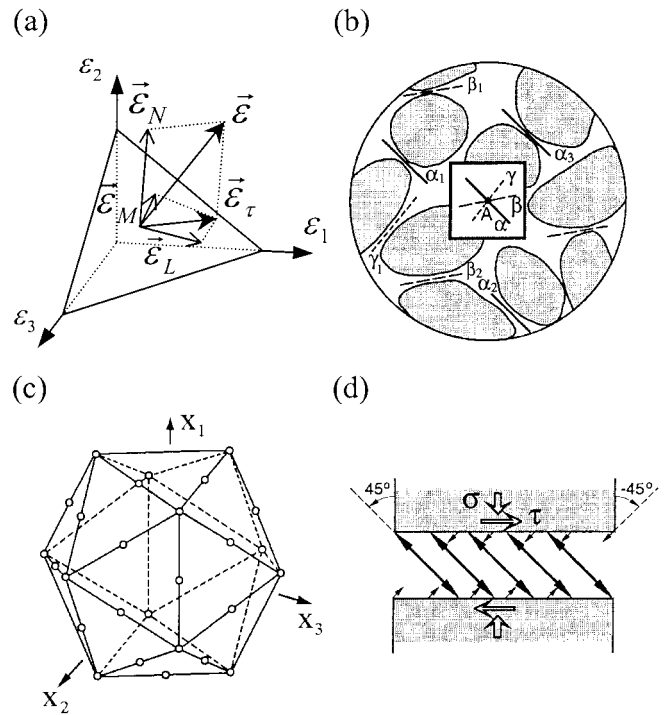


FIG. 1. (a) Microplane Model Ensuing by Separate Homogenization of Slips and Openings on Weak Planes $\alpha_1, \alpha_2, \dots$ of Various Orientations $\alpha, \beta, \gamma, \dots$ within Representative Volume of Material; (b) Explanation of Shear-Dilatant Cross Coupling Engendered by Interaction of Microplanes (after Bažant and Gamberova 1984); (c) Strain Components on Microplane; (d) Example of 21-Point Optimal Gaussian Integration Formula (Circled Points at Vertices and Midedges of Icosahedron Represent Directions of Microplane Normals; Optimal Weights Were Calculated in Bažant and Oh 1996)

$$\epsilon_M = M_{ij}\epsilon_{ij}; \quad \epsilon_L = L_{ij}\epsilon_{ij} \quad (2a,b)$$

in which $M_{ij} = (m_i n_j + m_j n_i)/2$ and $L_{ij} = (l_i n_j + l_j n_i)/2$ (Bažant and Prat 1988a,b).

Because of the foregoing kinematic constraint relating the strains on the microlevel (microplane) and macrolevel (continuum), the static equivalence (or equilibrium) of stresses between the macro and micro levels can be enforced only approximately. This is done by the principle of virtual work (Bažant 1984) written for surface Ω of a unit hemisphere;

$$\frac{2\pi}{3} \sigma_{ij} \delta \epsilon_{ij} = \int_{\Omega} (\sigma_N \delta \epsilon_N + \sigma_L \delta \epsilon_L + \sigma_M \delta \epsilon_M) d\Omega \quad (3)$$

This equation means that the virtual work of macrostresses (continuum stresses) within a unit sphere must be equal to the virtual work of microstresses (microplane stress components) regarded as the tractions on the surface of the sphere. The integral physically represents a homogenization of different contributions coming from planes of various orientations within the material as depicted in Fig. 1(b) [for a detailed physical justification, see Bažant et al. (1996a)]. Substituting $\delta \epsilon_N = N_{ij} \delta \epsilon_{ij}$, $\delta \epsilon_L = L_{ij} \delta \epsilon_{ij}$ and $\delta \epsilon_M = M_{ij} \delta \epsilon_{ij}$, and noting that the last variational equation must hold for any variation $\delta \epsilon_{ij}$, one gets the following basic equilibrium relation (Bažant 1984):

$$\sigma_{ij} = \frac{3}{2\pi} \int_{\Omega} s_{ij} d\Omega \approx 6 \sum_{\mu=1}^{N_m} w_{\mu} s_{ij}^{(\mu)}$$

$$\text{with } s_{ij} = \sigma_N N_{ij} + \sigma_L L_{ij} + \sigma_M M_{ij} \quad (4)$$

As indicated, the integral in numerical calculations is approximated by an optimal Gaussian integration formula for a spher-

ical surface (Stroud 1971; Bažant and Oh 1986) representing a weighted sum over the microplanes of orientations \vec{n}_μ , with weights w_μ normalized so that $\sum_\mu w_\mu = 1/2$ (Bažant and Oh 1985, 1986). The most efficient formula that still yields acceptable accuracy involves 21 microplanes [Bažant and Oh (1986); Fig. 1(c)]. In explicit dynamic finite-element programs, integral (4) must be evaluated at each integration point of each finite element in each time step. The values of $N_{ij}^{(\mu)}$, $M_{ij}^{(\mu)}$, and $L_{ij}^{(\mu)}$ for all the microplanes $\mu = 1, \dots, N$ are common to all integration points of all finite elements and are calculated and stored in advance.

The most general explicit constitutive relation on the microplane level may be written as

$$\sigma_N(t) = \mathcal{F}'_{t=0}[\varepsilon_N(\tau), \varepsilon_M(\tau), \varepsilon_L(\tau)] \quad (5a)$$

$$\sigma_L(t) = \mathcal{G}'_{t=0}[\varepsilon_N(\tau), \varepsilon_M(\tau), \varepsilon_L(\tau)] \quad (5b)$$

$$\sigma_M(t) = \mathcal{H}'_{t=0}[\varepsilon_N(\tau), \varepsilon_M(\tau), \varepsilon_L(\tau)] \quad (5c)$$

where \mathcal{F} , \mathcal{G} , and \mathcal{H} are functionals of the history of the microplane strains in time t . Despite our avoidance of tensors, the number of possibilities is enormous. Lacking a complete micromechanical model, one must partly rely on intuitive understanding of the physical mechanism involved. To a large extent, this is an art.

MICRO-MACRO WORK CONJUGACY OF VOLUMETRIC-DEVIATORIC SPLIT

Although not absolutely necessary, it is very helpful for intuitive understanding to define the deviatoric strains on the microplanes:

$$\varepsilon_D = \varepsilon_N - \varepsilon_V; \quad \varepsilon_V = \varepsilon_{kk}/3 \quad (6a,b)$$

where ε_V = volumetric strain (mean strain), the same as for all the microplanes. Defining ε_S = spreading strain (or lateral strain) = mean normal strain in the lateral directions lying in the microplane, the volume change may be written as $3(\varepsilon_N - \varepsilon_D) = \varepsilon_N + 2\varepsilon_S$, which clarifies the physical meaning

$$\varepsilon_D = \frac{2}{3}(\varepsilon_N - \varepsilon_S) \quad (7)$$

The question now is how to define the volumetric and deviatoric stresses σ_V and σ_D on the microplanes. It will be convenient to use the work-conjugate volumetric stress, that is, such a stress that $\sigma_V \delta \varepsilon_V$ would be the correct work expression. So we define the volumetric stress on the microplanes by the variational equation

$$\frac{2\pi}{3} \frac{\sigma_{kk}}{3} \delta \varepsilon_{mm} = \int_{\Omega} \sigma_V \delta \varepsilon_V d\Omega \quad (8)$$

Substituting $\delta \varepsilon_V = \delta \varepsilon_{kk}/3$ and noting that $\int_{\Omega} d\Omega = 2\pi$, we obtain for the volumetric stress on the microplanes:

$$\sigma_V = \sigma_{kk}/3 \quad (9)$$

Subtracting (8) from (3), we get

$$\frac{2\pi}{3} \left(\sigma_{ij} - \frac{\sigma_{kk}}{3} \delta_{ij} \right) \delta \varepsilon_{ij} = \int_{\Omega} [\sigma_D \delta \varepsilon_D + \sigma_D \delta \varepsilon_V + \sigma_V \delta \varepsilon_D + \sigma_L \delta \varepsilon_L + \sigma_M \delta \varepsilon_M] d\Omega \quad (10)$$

where $\sigma_D = \sigma_N - \sigma_V$ and $\delta \varepsilon_D = \delta \varepsilon_N - \delta \varepsilon_V$. Noting that the deviatoric stress tensor $\sigma_{ij}^D = \sigma_{ij} - (\sigma_{kk}/3)\delta_{ij}$, and that $\int_{\Omega} \sigma_D \delta \varepsilon_V d\Omega = \int_{\Omega} \sigma_V \delta \varepsilon_D d\Omega = 0$, we have

$$\sigma_{ij}^D \delta \varepsilon_{ij} = \frac{3}{2\pi} \int_{\Omega} (\sigma_D \delta \varepsilon_D + \sigma_L \delta \varepsilon_L + \sigma_M \delta \varepsilon_M) d\Omega \quad (11)$$

The kinematic constraint means that the microstrains (a short for the strain tensor components on the microplane) are calculated as the projections of the strain tensor (macrostrain). So, we have $\delta \varepsilon_N = N_{ij} \delta \varepsilon_{ij}$, which leads to $\delta \varepsilon_D = \delta \varepsilon_N - \delta \varepsilon_V = (N_{ij} - \delta_{ij}/3) \delta \varepsilon_{ij}$ and $\delta \varepsilon_L = L_{ij} \delta \varepsilon_{ij}$ with $\delta \varepsilon_M = M_{ij} \delta \varepsilon_{ij}$. Substitution of these relations into (11) and addition of the volumetric strain yield the result:

$$\sigma_{ij} = \sigma_V \delta_{ij} + \sigma_{ij}^D \quad (12a)$$

$$\sigma_{ij}^D = \frac{3}{2\pi} \int_{\Omega} \left[\sigma_D \left(N_{ij} - \frac{\delta_{ij}}{3} \right) + \sigma_L L_{ij} + \sigma_M M_{ij} \right] d\Omega \quad (12b)$$

With the volumetric-deviatoric split, the elastic stress-strain relations on the microplanes may be written in the rate form as

$$\dot{\sigma}_V = E_V \dot{\varepsilon}_V; \quad \dot{\sigma}_D = E_D \dot{\varepsilon}_D; \quad \dot{\sigma}_M = E_T \dot{\varepsilon}_M; \quad \dot{\sigma}_L = E_T \dot{\varepsilon}_L \quad (13a-d)$$

where E_V , E_D , and E_T = microplane elastic moduli whose relationship to the macroscopic Young's modulus E and Poisson ratio ν is $E_V = E/(1 - 2\nu)$; $E_D = 5E/[(2 + 3\mu)(1 + \nu)]$; and $E_T = \mu E_D$ (Bažant and Prat 1988a,b); here μ = parameter that may be chosen. It is best chosen as $\mu = 1$ (Bažant et al. 1996a). The reasons: (1) It makes it possible to characterize damage by a purely geometric fourth-rank damage tensor (a tensor independent of the material stiffness properties); and (2) it causes the so-called "true" microplane stresses ("true" in the sense of continuum damage mechanics) to obey a static constraint to the macroscopic true stress tensor (Carol et al. 1991; Carol and Bažant 1997).

The term $-\delta_{ij}/3$ in (12) was absent from the previous versions of the microplane model. This term (the need for which was established in Carol et al. 1998) ensures that always $\sigma_{kk}^D = 0$, even when $\int_{\Omega} \sigma_D d\Omega \neq 0$.

For purely elastic deformations, $\int_{\Omega} \sigma_D d\Omega = 0$, and so this term has no effect on the values of σ_{ij}^D . The reason is that

$$\int_{\Omega} (E_D \varepsilon_D) \frac{\delta_{ij}}{3} d\Omega = - \int_{\Omega} E_D \left(n_{kn} - \frac{\delta_{kl}}{3} \right) \varepsilon_{kl} \frac{\delta_{ij}}{3} d\Omega = 0 \quad (14)$$

where $\int_{\Omega} n_{kn} d\Omega = (2\pi/3)\delta_{kl}$.

For inelastic deformations, though, $\int_{\Omega} \sigma_D d\Omega \neq 0$, and so the term $-\delta_{ij}/3$ in (12b) does have an effect. In the special case that the tensile and compressive stress-strain boundaries (strain-dependent yield limits) on the deviatoric strain are symmetric or nearly symmetric, the effect of this term on σ_{ij}^D is very small (but generally nonzero).

It is interesting that if a 2D (planar) microplane model with symmetric tensile and compressive boundaries were considered, this term would have no effect at all. This is clear by considering the Mohr circle for a 2D deviatoric strain. Two mutually orthogonal microplanes correspond on the circle to normal strains of equal magnitude and opposite sign, and so the contributions of the corresponding stresses must cancel each other if the tensile and compressive boundaries are symmetric. In three dimensions, though, the symmetry of the boundaries only mitigates the effect of this term but does not suffice to wipe it out, as can be checked by simple numerical examples.

The stronger the asymmetry of the tensile and compressive deviatoric boundaries, the greater is the effect of the new term $-\delta_{ij}/3$ in (12b) on σ_{ij}^D . This makes it possible to exploit the asymmetry of the tensile and compressive deviatoric boundaries for controlling dilatancy and pressure sensitivity of deviatoric deformations [Fig. 1(d)]. In the previous microplane model M3, the absence of the term $-\delta_{ij}/3$ had to be compensated by empirical dependence of deviatoric deformations on σ_V , which can now be omitted.

The absence of the term $-\delta_{ij}/3$ in (12b) from model M2

and M3 can cause violations of thermodynamic restrictions, particularly negative dissipation during a closed strain cycle (Carol et al. 1999). Such violations can be significant for model M2, but are negligible for model M3, for two reasons: (1) The volume change, being limited by the normal and volumetric boundaries, is always small; and (2) the compressive and tensile deviatoric boundaries are almost symmetric in M3.

MICROPLANE MODELING OF INELASTIC BEHAVIOR

The constitutive model will now be defined on the microplane level. All the material parameters except the standard cylindrical compression strength f'_c and Young's elastic modulus E are dimensionless. They are divided into the fixed (hard-to-adjust, constant) parameters, which are denoted as c_1, c_2, \dots, c_{17} and may be taken as the same for all concretes, and the free (easy-to-adjust) parameters, which are denoted as k_1, k_2, k_3, k_4 and reflect the differences between various concretes. Their roles and identification will be discussed in the next section.

As introduced in model M3, all the inelastic behavior is characterized by the so-called stress-strain boundaries on the microplane level. These boundaries may be regarded as strain-dependent yield limits. In general, they exhibit strain softening [in detail, see Bažant et al. (1996a)]. Within the boundaries, the response is incrementally elastic, although the elastic moduli may undergo progressive degradation as a result of damage. Exceeding the boundary stress is never allowed. Travel along the boundary is permitted only if the strain increment is of the same sign as the stress; otherwise, elastic unloading occurs. These simple rules for the boundaries suffice to obtain on the macrolevel the Bauschinger effect, as well as realistic hysteresis loops during cyclic loading. Despite the abrupt drop of slope when the stress reaches the boundary, the macroscopic response is quite smooth, thanks to the fact that different microplanes enter the unloading and reloading regime at different times.

Experience with data fitting has shown that the stress at each of the normal, volumetric, and deviatoric boundaries can be assumed to depend only on its conjugate strain, that is, the boundary stress σ_N depends only on ϵ_N , σ_V only on ϵ_V , and σ_D only on ϵ_D (Fig. 2). Apparently, the inelastic cross effects between nonconjugate strain and stress components on the macroscale (e.g., between σ_{11} and ϵ_{22} or ϵ_{12}) are adequately captured by interactions among various microplanes engendered by the kinematic constraint. A few boundaries are strain independent, and thus they degenerate into yield surfaces. This is the case, for example, for the shear boundary, which describes frictional interaction between two different stress components—the normal stress and the shear stress [Fig. 2(A and a)].

Horizontal Boundaries (Yield Surfaces)

In the previous models M1 and M2, a smoothly curved inelastic stress-strain relation was introduced on the microplane. Although cross dependencies between nonassociated components were avoided, this was somewhat unwieldy and did not allow independently controlling the peak stress and the steepness of postpeak descent. Furthermore, in model M3, the adoption of the simple concept of stress-strain boundaries, with a sudden transition from elastic behavior inside the boundary to softening on the boundary, caused the peaks of the macroscopic response curve to be too sharp compared to the test data (the data generally display smooth rounded peaks).

These shortcomings are remedied in the present model M4. The roundness of the stress peaks in unconfined compression and in tension suggests the existence of a certain limited capacity for yield. To capture it, the present model features ad-

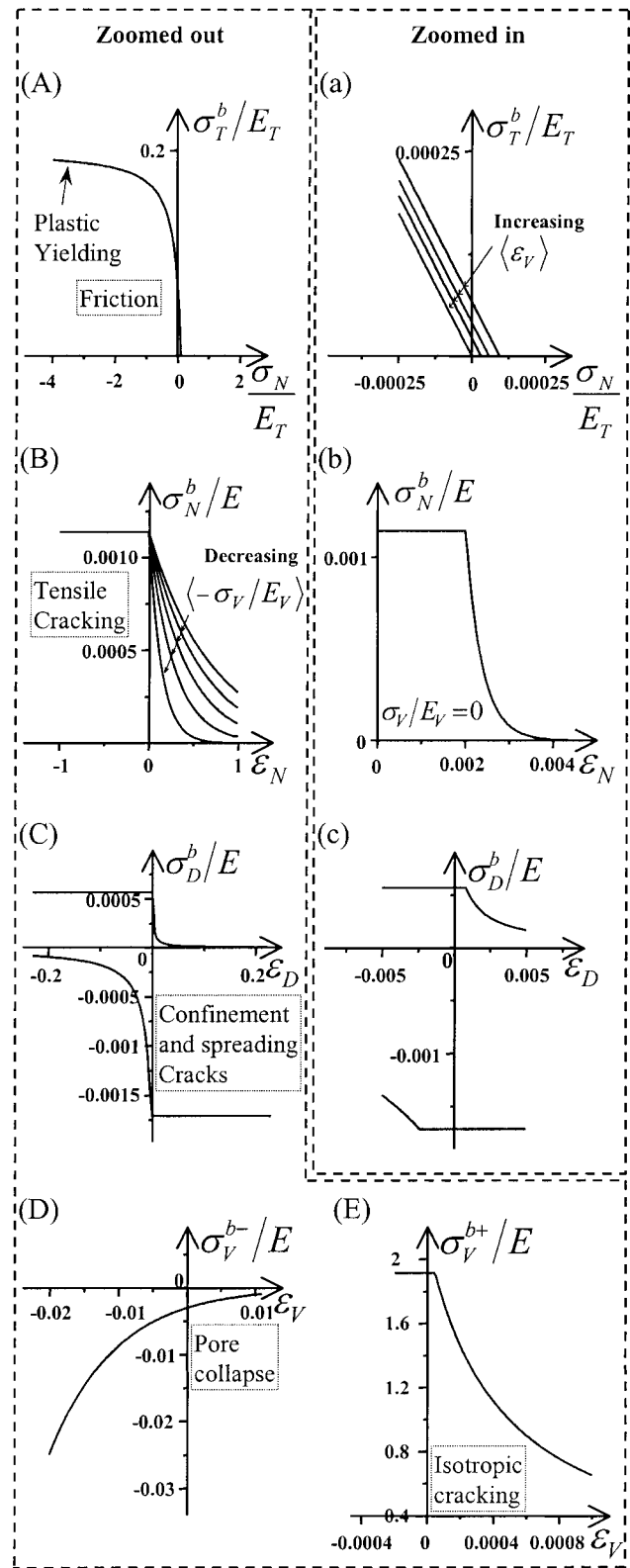


FIG. 2. (A, B, C, D, E) Stress-Strain Boundaries Plotted at Large Scales; (a, b, c) Boundaries from (A, B, C) Replotted at Small Scales (for $E = 25$ GPa and Reference Values $k_1 = 0.000245, k_2 = 110, k_3 = 12, k_4 = 36$)

ditional horizontal boundaries for the tensile normal stress and the tensile and compressive deviatoric stresses on the microplanes [Figs. 2(B), (C), (b), and (c)]. These additional boundaries are strain independent and represent microplane yield limits.

In contrast to the softening boundaries used exclusively in

M3, the additional horizontal boundaries (yield limits) give a very different distribution of the inelastic strains over the microplanes. When the softening boundary becomes active, all the inelastic strains tend to localize into very few microplanes, even into just one of them, while most microplanes unload. On the other hand, for the horizontal boundaries, such localization among spatial orientations does not take place; rather, the yielding gradually spreads over many microplanes, and no microplanes unload. The capacity of simultaneous yielding (but not simultaneous softening) of many microplanes causes the peak of the stress-strain curve to be smoothly curved, even though the transition from elasticity to yielding on the microplane is sudden. By extending the range of the horizontal boundaries, it is possible to generate a plateau of any length on the macroscopic stress-strain curves.

Imposition of separate horizontal boundaries (yield limits) further improves the hysteretic loops under cyclic loading. After a loading cycle, the stress-strain path goes from the elastic regime into the leftward extension of the horizontal boundary and then follows that boundary until the softening boundary is reached (Fig. 2). In M3, the microplane stress-strain path went, after a load cycle, from the elastic regime directly into the steep softening boundary (which was extended leftward to high stress values). This caused the peaks of the hysteretic loops to be too high and too sharp.

Normal Stress Boundaries (Tensile Cracking, Fragment Pullout, Crack Closing)

In the original model M1, the macroscopic tensile strain softening was controlled on the microplane level of strain softening of the normal stress, which worked perfectly. In model M2, this was replaced by separate strain softening of the volumetric and deviatoric stress components on the microplane. In retrospect, this was not surprising because there were two independent simultaneous softening processes, in which case the strain softening must be expected to localize into one of them (Bažant and Cedolin 1991). It did localize into the volumetric softening while the deviatoric stress unloaded, thus causing excessive lateral expansion, as discovered by M. Jirásek (1993). No similar problem occurred in compression because only one component, the deviatoric one, underwent strain softening in model M2, while the other, volumetric one did not.

In model M3, in which the concept of stress-strain boundary was introduced (chiefly to facilitate the handling of hysteresis), this problem was corrected by controlling the tensile strain softening through a strain-softening boundary on the total normal stress component on each microplane, which was the same as in M1. The normal stress boundary was imposed in addition to deviatoric boundaries. This successful aspect of model M3 is retained here. The tensile normal boundary is given as

$$\sigma_N^b = F_N(\epsilon_N) = Ek_1c_1 \exp\left(-\frac{\langle\epsilon_N - c_1c_2k_1\rangle}{k_1c_3 + \langle -c_4(\sigma_V/E_V)\rangle}\right) \quad (15)$$

where subscript b refers to the stress at the boundary; parameter c_3 controls mainly the steepness of the postpeak slope in uniaxial tension. The Macaulay brackets, defined as $\langle x \rangle = \text{Max}(x, 0)$, are used here and in several subsequent formulas to define horizontal segments of the boundaries, representing yield limits. The normal boundary in small and large ranges of normal strain is shown in Fig. 2(B and b). Physically, its initial descending part characterizes the tensile cracking parallel to the microplane, while its tail characterizes the frictional pullout of fragments and aggregate pieces bridging the crack from one of its faces.

In addition, the closing of cracks after tensile unloading needs to be represented by a crack-closing boundary, defined

simply as $\sigma_N^b = 0$ for $\epsilon_N > 0$; it prevents entry of the quadrant of positive ϵ_N and negative σ_N on the microplane level (although in terms of uniaxial stress on the macrolevel, this quadrant can be entered because of microplane interactions and deviatoric stresses).

Deviatoric Boundaries (Spreading, Splitting)

The compressive deviatoric boundary controls the axial crushing strain of concrete in compression when the lateral confinement is too weak to prevent crushing. The tensile deviatoric boundary simulates the transverse crack opening of axial distributed cracks in compression and controls the volumetric expansion and lateral strains in unconfined compression tests. Both boundaries have similar shapes and similar mathematical forms:

$$\text{for } \sigma_D > 0: \sigma_D^b = F_D^+(\epsilon_D) = \frac{Ek_1c_5}{1 + (\langle\epsilon_D - c_5c_6k_1\rangle/k_1c_18c_7)^2} \quad (16)$$

$$\text{for } \sigma_D < 0: \sigma_D^b = F_D^-(\epsilon_D) = -\frac{Ek_1c_8}{1 + (\langle -\epsilon_D - c_8c_9k_1\rangle/k_1c_7)^2} \quad (17)$$

In the previous model M3, the tensile deviatoric boundary was too high. This caused the lateral expansion in postpeak softening response under uniaxial compression to be much too high (almost double the measured expansion). The deviatoric boundaries in small and large ranges on normal strain are shown in Fig. 2(C and c). Because $\epsilon_D = (2/3)(\epsilon_N - \epsilon_S)$, the deviatoric boundaries physically characterize the splitting cracks normal to the microplane, caused by lateral spreading, and their prevention by lateral confinement.

Frictional Yield Surface

The shear boundary physically represents friction. It is a nonlinear frictional yield condition consisting of a dependence of the shear yield stress $\sigma_T = \sqrt{\sigma_L^2 + \sigma_M^2}$ on the normal stress σ_N [Fig. 2(A and a)]. Properly, a frictional boundary should be applied to the resultant shear stress $\vec{\sigma}_T$. Alternatively, to reduce the computational burden, the frictional boundary can be applied, not to the resultant shear stress $\vec{\sigma}_T$, but to the components σ_L and σ_M separately. In the latter case, a circular yield surface $\sigma_T = \text{const.}$ is replaced by a square yield surface in the (σ_L, σ_M) plane. The drawback is that the resultant shear stress at yield varies between σ_T and $\sigma_T\sqrt{2}$, depending on the random choice of L and M directions, which represents a certain infringement on the objectivity of modeling. On the macro-scale, however, the effects of the random choices of L and M directions average out, and almost the sole consequence is that the actual shear yield stress in terms of σ_T is, on the average, 11% higher than the shear yield stress imposed in terms of σ_L and σ_M [because $\int_0^{\pi/4} \cos \alpha \, d\alpha / (\pi/4) = 1.11$]. The latter is also more sensitive to rigid-body rotations of the integration points on the unit hemisphere than the former.

In the previous model M3, the frictional yield condition consisted of a linear relationship (proportionality) between the shear and normal stresses on the microplane. Such proportionality, however, gives far too high stresses in the case of very high hydrostatic pressures.

The new frictional boundary is nonlinear. It is a hyperbola starting with a finite slope at a certain finite distance from the origin of the tensile normal stress axis. This distance is gradually reduced to zero, with increasing damage quantified by the volumetric strain. Thus, when the volumetric strain is small, the boundary provides a finite cohesive stress, which then decreases to zero with increasing volumetric strain.

As the compressive stress magnitude increases, it approaches a horizontal asymptote. With this feature, the triaxial compression test data can be fitted more easily and closely

[not only for the classical data, but also for the recent U.S. Army Engineer Waterways Experiment Station (WES) data cited later]. A vertically shifted parabola with a horizontal axis and a dependence of the frictional shear stress on the volumetric rather than tensile stress, which was used in M3, has also been tried, but with less satisfactory results.

The distinction between virgin loading and repeated loading, which was used in M3 to make the response for initial virgin loading linearly elastic, is in the present model unnecessary because such response can be ensured by accounting for a finite cohesion value for small volumetric strains. The new friction boundary is expressed as

$$\sigma_T^b = F_T(-\sigma_N) = \frac{E_T k_1 k_2 c_{10} \langle -\sigma_N + \sigma_N^0 \rangle}{E_T k_1 k_2 + c_{10} \langle -\sigma_N + \sigma_N^0 \rangle} \quad (18)$$

where

$$\sigma_N^0 = \frac{E_T k_1 c_{11}}{1 + c_{12} \langle \epsilon_V \rangle} \quad (19)$$

If $\langle \epsilon_V \rangle$ is large, $c_{10} = [d\sigma_T/d\sigma_N]_{\sigma_N=0}$ = initial slope of the boundary, and $\lim_{\sigma_N \rightarrow \infty} \sigma_T = E_T k_1 k_2$, which represents a horizontal asymptote. Note that the foregoing expression involves a finite cohesion, which can be calculated by setting $\sigma_N = 0$, assuming $\epsilon_V < 0$. When $\epsilon_V \gg 0$, the friction boundary actually passes through the origin; hence the cohesion becomes zero. This is possible because the resistance to slip on one microplane at $\sigma_N = 0$ is provided by the normal stresses acting on other microplanes that are inclined with respect to that microplane. Because the shear stresses at the postpeak softening tail of the uniaxial (unconfined) compression test must lie on the frictional boundary (no unloading in shear), and all the microplane stresses must approach zero, a frictional boundary with zero cohesion (i.e., $\sigma_T = 0$ when $\sigma_N = 0$) is needed for making the axial stress at the tail approach zero. If the cohesion were finite (i.e., if $\sigma_T > 0$ when $\sigma_N = 0$), the tail would approach a finite asymptotic value in contradiction to experiments.

The existence of a horizontal asymptote means that, at very high confining pressures (larger than the standard compression strength), concrete becomes a plastic but frictionless material (the friction being characterized by the boundary slope at yield, which approaches 0). That this is indeed so has recently been confirmed by a new type of experiment—the so-called “tube-squash” test (Bažant et al. 1999)—in which a thick, highly ductile steel alloy tube is filled with concrete and squashed to about half of its initial length. Very high pressures develop, and shear angles above 70° are achieved in this test. Yet no cracks or voids are visible on a cut through the deformed material, and cohesion is not lost (the uniaxial compression strength of the cores drilled out from the deformed material is still about 30% of their virgin strength). Such plastic behavior occurs in concrete near the nose of a penetrating missile or explosively driven anchor.

Volumetric Boundaries (Pore Collapse, Expansive Breakup)

The inelastic behavior under hydrostatic pressure (as well as uniaxial compressive strain) exhibits no strain softening, but progressively stronger hardening caused primarily by collapse and closure of pores. It is simulated, the same as in M3, by a compressive volumetric boundary in the form of a rising exponential [Fig. 2(D)]. A tensile volumetric boundary needs to be imposed, too. These boundaries are

$$\text{for } \sigma_V < 0: \quad \sigma_V^b = F_V^-(\epsilon_V) = -E k_1 k_3 \exp\left(-\frac{\epsilon_V}{k_1 k_4}\right) \quad (20)$$

$$\text{for } \sigma_V > 0: \quad \sigma_V^b = F_V^+(\epsilon_V) = \frac{E_V k_1 c_{13}}{[1 + (c_{14}/k_1) \langle \epsilon_V - k_1 c_{13} \rangle]^2} \quad (21)$$

Although some data (particularly WES data) would be better fitted by a bilinear boundary, the exponential boundary better fits the majority of data.

Data fitting showed that the normal tensile boundary (15) alone cannot prevent unreasonable lateral strains in postpeak softening under uniaxial (unconfined) tension. Without the tensile volumetric boundary shown in Fig. 2(E), the slipping on microplanes inclined by about 45° can make an excessive contribution to axial extension, and since this slipping occurs at no change of volume, the material wants to develop transverse contraction, possibly very large. This is resisted by elastic volumetric stresses and can be prevented only by limiting these stresses with a tensile volumetric boundary. The tensile normal boundary cannot prevent this because the total axial tensile strain may still remain below that boundary, being offset by a negative deviatoric strain of large magnitude in the axial direction, caused by the slipping on inclined planes. That explains the need for the tensile volumetric boundary (21), whose physical meaning may be seen as an expansive breakup (due to cracking in all directions caused by volume expansion).

Unloading and Stiffness Degradation

The effect of closing of tensile cracks has already been described by the crack-closing boundary for normal stress. Furthermore, to model unloading, reloading, and cyclic loading with hysteresis, it is necessary to take into account the effect of material damage on the incremental elastic stiffness. The unloading can be defined in the microplane model separately for each strain component on the microplane, that is, some of ϵ_V , ϵ_D , and ϵ_T may be unloading, while others may be loading or reloading. The unloading criterion for any component is the negativeness of the work of that stress component. Thus unloading occurs if the sign of

$$\sigma_V \Delta \epsilon_V, \quad \sigma_D \Delta \epsilon_D, \quad \sigma_T \Delta \epsilon_T \quad (22)$$

becomes negative. This means that work is being recovered from the material by that strain component during unloading.

For virgin loading as well as reloading of any component, the incremental (tangential) moduli are constant and equal to the initial elastic moduli E_V , E_D , and E_T , with the exception of compressive hydrostatic reloading. As experiments show, the response in such reloading never returns to the virgin loading curve given by the compressive hydrostatic boundary. After the reloading straight line of slope E_V becomes parallel to the boundary slope for the same ϵ_V , the response moves parallel to the boundary curve; this may be described as $E_V^{\text{reloaded}} = \max[E_V, dF_V^-(\epsilon_V)/d\epsilon_V]$.

Unloading is assumed to occur when the work rate $\sigma \dot{\epsilon}$ (or increment $\sigma \Delta \epsilon$) becomes negative, and this unloading criterion is considered separately for each microplane stress component. The following empirical rules for the incremental unloading moduli on the microplanes have been developed, with good results:

for $\epsilon_V \leq 0$ and $\sigma_V \leq 0$:

$$E_V^U(-\epsilon_V, -\sigma_V) = E_V \left(\frac{c_{15}}{c_{15} - \epsilon_V} + \frac{\sigma_V}{c_{15} c_{16} E_V} \epsilon_V \right) \quad (23)$$

for $\epsilon_V > 0$ and $\sigma_V > 0$:

$$E_V^U(\epsilon_V, \sigma_V) = \min[\sigma_V(\epsilon_V)/\epsilon_V, E_V] \quad (24)$$

$$E_D^U = (1 - c_{17})E_D + c_{17}E_D^S \quad (25)$$

$$\text{where if } \sigma_D \epsilon_D \leq 0: E_D^S = E_D, \quad \text{else } E_D^S = \min(\sigma_D/\epsilon_D, E_D) \quad (26)$$

$$E_T^U = (1 - c_{17})E_T + c_{17}E_T^S \quad (27)$$

where if $\sigma_T \varepsilon_T \leq 0$: $E_T^S = E_T$, else $E_T^S = \min(\sigma_T/\varepsilon_T, E_T)$ (28)

here c_{15} , c_{16} , c_{17} = fixed dimensionless parameters, and super-script S denotes the secant modulus; c_{17} controls the unloading modulus, which would be the virgin elastic modulus for $c_{17} = 0$, and the secant modulus for $c_{17} = 1$. The values $c_{15} = 0.02$, $c_{16} = 0.01$, and $c_{17} = 0.4$ were found to work well.

Eq. (23) for hydrostatic compression reflects the experimental observation that, for unloading that starts from some pressure much higher than the uniaxial compression strength, the unloading slope is initially higher than the virgin bulk elastic modulus but becomes smaller than that after the pressure has been reduced much below the uniaxial compression strength.

The property that one microplane strain component may be unloading while another is loading is an advantage compared to the classical theory of plasticity. Such behavior is admissible because the microplane stress and strain components are not tensors and thus do not have to satisfy any tensorial invariance conditions. When some microplane strains on some microplane are unloading, while other microplane strains on the same microplane or another microplane are simultaneously loading (or reloading), residual stresses balancing each other (with a zero macroscopic resultant σ_{ij}) are being accumulated and locked up in the kinematically constrained microplane system. Their strain energy is thus also being locked up and accumulated. This simulates accumulation of strain energy in the microstructure of material, which is known to be the physical source of fatigue. Thus it transpires that the microplane model ought also to be effective for a physically realistic modeling of fatigue based on the energy stored in residual stresses, although checking this aspect is beyond the scope of this study.

CLOSING COMMENT

The behavior of concrete under uni-, bi-, and triaxial loadings displays a rich assortment of diverse characteristic features. The range of various types of multiaxial test data is probably broader than for any other materials. Consequently, the optimal fitting of test data and calibration of model coefficients is the most difficult task in the development of a microplane model for concrete. This task, as well as the numerical algorithm and formulation of conclusions, is left for the second part of this study (Caner and Bažant 2000).

APPENDIX I. ADVANTAGES AND BASIC FEATURES OF MICROPLANE MODEL

It might be useful to give the following summary of the advantages of microplane model compared to the classical tensorial models.

1. The constitutive law is written in terms of vectors rather than tensors. The modeler need not worry about tensorial invariance because it is automatically satisfied by combining the responses from microplanes of all possible orientations.
2. The inelastic physical phenomena associated with surfaces, such as slip, friction, tensile cracking, or lateral confinement on a given plane or its spreading, can be characterized directly in terms of the stress and strain on the surface on which they take place. This contrasts with tensorial models in which, for instance, a relation between the invariants I_1 and J_2 is regarded as friction, although it is only a poor overall measure of friction, unable to capture frictional slip on any particular plane.
3. In computational practice, macroscopic tensorial plastic-damage models with only one or two loading surfaces are generally used. For such models, most mate-

rials appear to exhibit large apparent deviations from the normality rule for the plastic strain increments. Aside from friction, the reason is that in reality many simultaneous yield (or loading) surfaces intersect at every point of a plastic loading path in the stress space [e.g., Bažant (1978, 1980)]. However, the classical multisurface plasticity proposed by Koiter in 1953 seems next to impossible to fit to more extensive test data. The microplane model is equivalent to infinitely many simultaneous (active or inactive) loading surfaces of all possible orientations, at least one for each microplane. This enables the model to automatically capture these apparent deviations from normality, including those caused by dilatancy in frictional slip (Bažant and Gambarova 1984).

4. Unlike the classical plasticity models used in computational practice, the microplane model captures the so-called vertex effect, that is, the fact that an apparent vertex (or corner) exists at every point of the yield surface detected by radial loading. In the classical models, the incremental stiffness for a loading increment parallel to this surface (called "loading to the side") is the initial elastic stiffness, but the real stiffness is much smaller, being close to the secant stiffness. Since several simultaneous loading surfaces are used on each microplane, and many exist among the set of microplanes, the vertex effect, that is, a reduced stiffness to the side (Bažant 1980), is automatically exhibited by the microplane model (F. C. Caner's ongoing, yet unpublished, tests show that the tangent torsional stiffness of a concrete cylinder uniaxially precompressed to strain -0.45% is only 35% of the initial elastic torsional stiffness, which is correctly predicted by the present microplane model, but not any plasticity model).
5. Extension to strain softening requires making the yield surfaces dependent on the strains. In the classical tensorial approach, this means that the yield surface in the stress space must parametrically depend on the invariants of the strain tensor. To this end, stress-bounding surfaces in the 18-dimensional space of all the components of σ_{ij} and ε_{ij} combined would need to be considered. In the microplane approach, it suffices that the yield limit for a microplane stress component be made to depend on only one strain component on that microplane.
6. The interaction of microplanes due to the kinematic constraint suffices to provide all the main cross effects on the macrolevel, such as the pressure sensitivity of inelastic shear strain and the dilatancy. It is therefore possible to use on the microplane level simple one-to-one stress-strain laws relating a stress component to its associated strain component, as data-fitting experience confirms (beginning with Bažant and Gambarova 1984) [Fig. 1(d)]. Microplane friction, though, is an exception—a yield surface in terms of two (but not more than two) microplane stress components is needed.
7. A vast number of combinations of loading or unloading on various microplanes is possible, and some microplanes unload even for monotonic loading on the macroscale. This is an important source of path dependence in the microplane model and allows simple yet physically realistic representation of the Bauschinger effect at reverse loading and of hysteresis under cyclic loading. The richness of these combinations makes possible the use of path-independent stress-strain relations for loading on each microplane.
8. During unload-reload cycles, residual stresses on microplanes (i.e., self-equilibrated stresses in balance with

a zero stress tensor of the continuum) are being automatically locked up within the microplane system, and their strain energy gradually accumulated, thus weakening the response. This naturally models fatigue, as well as hysteresis during cyclic loading.

9. With the microplane approach, anisotropic materials are not appreciably more difficult to model than isotropic materials. It suffices to use either orientation-dependent model parameters or an orientation-dependent weight function in the integral of the variational principle expressing the micro-macro relationship.
10. When the stress-strain boundaries on the microplanes include a horizontal segment (nonsoftening yield surface), the yielding spreads during loading over many microplanes and does so gradually (until some microplane enters a strain-softening regime, after which the inelastic behavior quickly localizes into only one or a few microplanes). This gradual spread of yielding over many microplanes automatically produces on the macrolevel a rising stress-strain curve with a gradually diminishing slope, even if the transition from elastic response to yielding on the microplanes is abrupt. So one need not bother with the modeling of strain hardening on the microplane level (unless some precise shape of hardening stress-strain curve is to be matched).
11. The philosophies of the microplane approach and finite elements blend well. While the latter represents a spatial discretization (with respect to distance), the former can be regarded as an angular discretization (with respect to orientations). In both, the principle of virtual work is used in analogous ways, suitable for explicit temporal integration. The microplane concept also blends well with the nonlocal concept. While the latter captures interactions of damage at distance, the former captures interactions among angular orientations. While the nonlocal integral of the latter prevents spurious localizations in space, the kinematic constraint of the former prevents spurious localizations among orientations (Bažant and Planas 1998, Sec. 14.1).
12. The inherent conceptual simplicity of the model, gained by dealing with stress and strain components rather than tensors and their invariants, facilitates understanding and intuition. This is important since modeling of complex materials is as much an art as a science.

The penalty to pay for these advantages is an increase in computational work and storage requirements, which is about 10-fold within the constitutive subroutine compared to the classical plasticity models. This is due to the need to deal with stress components on all the microplanes, whose number must be at least 21 for acceptable accuracy (Bažant and Oh 1996). This penalty, however, becomes relatively less burdensome for very large structural systems in which the computational work is dominated by solving the system rather than the material subroutine. Thanks to the rapid rise of computer power, the microplane model is no longer computationally forbidding. Concrete structures discretized with several millions of finite elements are being analyzed today at WES with the wave code (hydrocode) EPIC containing an explicit microplane constitutive subroutine developed at Northwestern.

An appealing aspect of the microplane model with a kinematic constraint is that it can be cast in the form of continuum damage mechanics. In that case, the damage variable is a fourth-order tensor, which represents the reduction of the stress-resisting cross-section area fraction in the material and is independent of microscopic material stiffness characteristics (Carol et al. 1991; Carol and Bažant 1997).

It may be noted that the microplane model is a necessary

consequence of mathematical homogenization (smearing) applied separately for various orientations. In concrete, the major contribution to inelastic strain comes from the slip and opening on weak planes within the microstructure, typically lying in the thin contact layers between aggregate pieces [Fig. 1(b)]. This slip and opening may be considered to conform kinematically to the strain of the macroscopic continuum at point *A* lying at the center of the representative volume of material [Fig. 1(c)]. One may now isolate within the representative volume of the material all the weak planes α_1 , α_2 , and α_3 whose normals have orientations with spherical coordinate angles between (ϕ, θ) and $(\phi + d\phi, \theta + d\theta)$. Macroscopic homogenization (smearing) of the slips and openings on the weak planes α_1 , α_2 , and α_3 yields a continuum that exhibits at point *A* the corresponding homogenized inelastic strains on plane α of the same orientation (ϕ, θ) . Considering all the possible orientations, one thus obtains by such separate homogenization processes a number of planes of many orientations [Fig. 1(c)], all of them located at *A* and all with strains constrained kinematically to the same continuum strain tensor.

Fig. 1(d) (after Bažant and Gambarova 1984) explains how the microplane model automatically generates dilatancy in shear. The shear strain in a band prevented from expanding causes normal tensile and compressive strains at microplanes inclined by $\pm 45^\circ$. Because the microplane strength of concrete is much smaller in tension than in compression, the compressive normal stress vectors on microplanes inclined by 45° are, at large shear strain, much larger than the tensile normal stress vectors on microplanes inclined by -45° , causing a large compressive normal stress resultant σ across the band. If this resultant is not opposed by a restraint against lateral expansion of the band, the band will expand. This represents dilatancy. Thus the constitutive law for a microplane need not involve any cross coupling between the normal stress and shear strain on a microplane.

APPENDIX II. REFERENCES

- Batdorf, S. B., and Budianski, B. (1949). "A mathematical theory of plasticity based on the concept of slip." *Tech. Note No. 1871*, National Advisory Committee for Aeronautics, Washington, D.C.
- Bažant, Z. P. (1978). "Endochronic inelasticity and incremental plasticity." *Int. J. Solids and Struct.*, 14, 691–714.
- Bažant, Z. P. (1980). "Work inequalities for plastic-fracturing materials." *Int. J. Solids and Struct.*, 16, 870–901.
- Bažant, Z. P. (1984). "Chapter 3: Microplane model for strain controlled inelastic behavior." *Proc., Mech. of Engrg. Mat.*, C. S. Desai and R. H. Gallagher, eds., Wiley, London, 45–59.
- Bažant, Z. P., and Cedolin, L. (1991). *Stability of structures: Elastic, inelastic, fracture and damage theories*, Oxford University Press, New York.
- Bažant, Z. P., and Gambarova, P. (1984). "Crack shear in concrete: Crack band microplane model." *J. Struct. Engrg.*, ASCE, 110(9), 2015–2035.
- Bažant, Z. P., and Kim, J.-K. (1986). "Creep of anisotropic clay: Microplane model." *J. Geotech. Engrg.*, ASCE, 112(4), 458–475.
- Bažant, Z. P., Kim, J.-H., and Brocca, M. (1999). "Finite strain tube-squash test for concrete at high pressure and shear angles up to 70° ." *ACI Mat. J.*, 96(5), 580–592.
- Bažant, Z. P., and Oh, B.-H. (1983). "Microplane model for fracture analysis of concrete structures." *Proc., Symp. on Interaction of Non-Nuclear Munitions with Struct.*, U.S. Air Force Academy, Colorado Springs, Colo., 49–53.
- Bažant, Z. P., and Oh, B.-H. (1985). "Microplane model for progressive fracture of concrete and rock." *J. Engrg. Mech.*, ASCE, 111(4), 559–582.
- Bažant, Z. P., and Oh, B.-H. (1986). "Efficient numerical integration on the surface of a sphere." *Zeitschrift für angewandte Mathematik und Mechanik (ZAMM)*, Berlin, 66(1), 37–49.
- Bažant, Z. P., and Ožbolt, J. (1990). "Nonlocal microplane model for fracture, damage, and size effect in structures." *J. Engrg. Mech.*, ASCE, 116(11), 2485–2505.
- Bažant, Z. P., and Ožbolt, J. (1992). "Compression failure of quasi-brittle material: Nonlocal microplane model." *J. Engrg. Mech.*, ASCE, 118(3), 540–556.

- Bažant, Z. P., and Planas, J. (1998). *Fracture and size effect in concrete and other quasibrittle materials*, CRC Press, Boca Raton, Fla.
- Bažant, Z. P., and Prat, P. C. (1987). "Creep of anisotropic clay: New microplane model." *J. Engrg. Mech.*, ASCE, 113(7), 1050–1064.
- Bažant, Z. P., and Prat, P. C. (1988a). "Microplane model for brittle-plastic material. I: Theory." *J. Engrg. Mech.*, ASCE, 114(10), 1672–1688.
- Bažant, Z. P., and Prat, P. C. (1988b). "Microplane model for brittle-plastic material. II: Verification." *J. Engrg. Mech.*, ASCE, 114(10), 1689–1699.
- Bažant, Z. P., Xiang, Y., Adley, M. D., Prat, P. C., and Akers, S. A. (1996b). "Microplane model for concrete. II: Data delocalization and verification." *J. Engrg. Mech.*, ASCE, 122(3), 255–262.
- Bažant, Z. P., Xiang, Y., and Prat, P. C. (1996a). "Microplane model for concrete. I: Stress-strain boundaries and finite strain." *J. Engrg. Mech.*, ASCE, 122(3), 245–254.
- Budianski, B., and Wu, T. T. (1962). "Theoretical prediction of plastic strains of polycrystals." *Proc., 4th U.S. Nat. Congr. of Appl. Mech.*, ASME, New York, 1175–1185.
- Caner, F. C., and Bažant, Z. P. (2000). "Microplane model M4 for concrete. II: Algorithm and calibration." *J. Engrg. Mech.*, ASCE, 126(9), 954–961.
- Carol, I., and Bažant, Z. P. (1997). "Damage and plasticity in microplane theory." *Int. J. Solids and Struct.*, 34(29), 3807–3835.
- Carol, I., Bažant, Z. P., and Prat, P. C. (1991). "Geometric damage tensor based on microplane model." *J. Engrg. Mech.*, 117(10), 2429–2448.
- Carol, I., Jirásek, M., Bažant, Z. P., and Steinmann, P. (1998). "New thermodynamic approach to microplane model with application to finite deformations." *Tech. Rep. PI-145*, International Center for Numerical Methods in Engineering (CIMNE), Barcelona, Spain.
- Carol, I., Jirásek, M., and Bažant, Z. P. (2000). "New thermodynamic approach to microplane model. Part I: Free energy and consistent microplane stresses." *Rep.*, Northwestern University, Evanston, Ill.
- Carol, I., Prat, P. C., and Bažant, Z. P. (1992). "New explicit microplane model for concrete: Theoretical aspects and numerical implementation." *Int. J. Solids and Struct.*, 29(9), 1173–1191.
- Cofer, W. F., and Kohut, S. W. (1994). "A general nonlocal microplane concrete material model for dynamic finite element analysis." *Comp. and Struct.*, 53(1), 189–199.
- Hasegawa, T., and Bažant, Z. P. (1993). "Nonlocal microplane concrete model with rate effect and load cycles. I: General formulation." *J. Mat. in Civ. Engrg.*, ASCE, 5(3), 372–393.
- Hill, R. (1965). "Continuum micromechanics of elastoplastic polycrystals." *J. Mech. Phys. Solids*, 13, 89–101.
- Hill, R. (1966). "Generalized constitutive relations for incremental deformations of metal crystals by multi-slip." *J. Mech. Phys. Solids*, 14, 95–102.
- Jirásek, M. (1993). "Modeling of fracture and damage in quasibrittle materials." PhD dissertation, Northwestern University, Evanston, Ill.
- Kröner, E. (1961). "Zur plastischen Verformung des Vielkristalls." *Acta Metallurgica*, 9(Feb.), 155–161.
- Kuhl, E., and Carol, I. (2000). "New thermodynamic approach to microplane model. I: Dissipation and inelastic constitutive modeling." *Int. J. Solids and Struct.*, in press.
- Lin, T. H., and Ito, M. (1965). "Theoretical plastic distortion of a polycrystalline aggregate under combined and reversed stresses." *J. Mech. Phys. Solids*, 13, 103–115.
- Lin, T. H., and Ito, M. (1966). "Theoretical plastic stress-strain relationship of a polycrystal." *Int. J. Engrg. Sci.*, 4, 543–561.
- Ožbolt, J., and Bažant, Z. P. (1992). "Microplane model for cyclic triaxial behavior of concrete and rock." *J. Engrg. Mech.*, ASCE, 118(7), 1365–1386.
- Ožbolt, J., and Bažant, Z. P. (1996). "Numerical smeared fracture analysis: Nonlocal microcrack interaction approach." *Int. J. Numer. Methods in Engrg.*, Chichester, U.K., 39, 635–661.
- Pande, G. N., and Sharma, K. G. (1981). "Time-dependent multi-laminate model for clay—a numerical study of the influence of rotation of principal stress axes." *Proc., Implementation of Comp. Procedures and Strain-Stress Laws in Geotech. Engrg.*, Vol. II, Acorn Press, Durham, N.C., 575–590.
- Pande, G. N., and Sharma, K. G. (1982). "Multi-laminate model of clays—A numerical evaluation of the influence of rotation of the principal stress axis." *Rep.*, Dept. of Civ. Engrg., University College of Swansea, U.K.
- Pande, G. N., and Xiong, W. (1982). "An improved multi-laminate model of jointed rock masses." *Proc., Int. Symp. on Numer. Models in Geomech.*, R. Dungar, G. N. Pande, and G. A. Studder, eds., Balkema, Rotterdam, The Netherlands, 218–226.
- Prat, P. C., and Bažant, Z. P. (1991). "Microplane model for triaxial deformation of saturated cohesive soils." *J. Geotech. Engrg.*, ASCE, 117(6), 891–912.
- Prat, P. C., Sánchez, F., and Gens, A. (1997). "Equivalent continuum anisotropic model for rocks: Theory and application to finite-element analysis." *Proc., 6th Int. Symp. on Numer. Methods in Geomech.*, Balkema, Rotterdam, The Netherlands, 159–166.
- Rice, J. R. (1970). "On the structure of stress-strain relations for time-dependent plastic deformation of metals." *J. Appl. Mech.*, 37(Sept.), 728–737.
- Stroud, A. H. (1971). *Approximate calculation of multiple integrals*, Prentice-Hall, Englewood Cliffs, N.J.
- Taylor, G. I. (1938). "Plastic strain in metals." *J. Inst. of Metals*, London, 62, 307–324.
- Zienkiewicz, O. C., and Pande, G. N. (1977). "Time-dependent multi-laminate model of rocks—A numerical study of deformation and failure of rock masses." *Int. J. Numer. and Analytical Methods in Geomech.*, 1, 219–247.